PHYSICAL REVIEW B, VOLUME 63, 020402(R)

Mesoscale magnetism at the grain boundaries in colossal magnetoresistive films

Yeong-Ah Soh,[1] G. Aeppli,[1] N. D. Mathur,[2] and M. G. Blamire[2]
[1]*NEC Research Institute, 4 Independence Way, Princeton, New Jersey 08540*
[2]*Department of Materials Science, University of Cambridge, Cambridge CB2 3QZ, United Kingdom*
(Received 6 October 2000; published 20 December 2000)

We report mesoscale regions with distinctive magnetic properties in epitaxial $La_{1-x}Sr_xMnO_3$ films which exhibit tunneling-like magnetoresistance across grain boundaries. By using temperature-dependent magnetic force microscopy we observe that the mesoscale regions are formed near the grain boundaries and have a different Curie temperature (up to 20 K *higher*) than the grain interiors. Our images provide direct evidence for previous speculations that the grain boundaries in thin films are not magnetically and electronically sharp interfaces. The size of the mesoscale regions varies with temperature and nature of the underlying defect.

DOI: 10.1103/PhysRevB.63.020402 PACS number(s): 75.70.Kw

Since the observation of large low-field magnetoresistance in polycrystalline $La_{1-x}A_xMnO_3$ (A=Ba,Ca,Sr),[1–4] where the effect was attributed to domain-wall scattering or spin-polarized tunneling between grains, much attention has been drawn to the role of grain boundaries (GB's) in the magnetotransport of manganites.[5–7] To isolate the grain boundary contribution to magnetotransport, mesoscopic devices were patterned on $La_{1-x}A_xMnO_3$ films grown on bicrystal substrates with an artificial grain boundary.[8–10] Despite evidence that the grain boundaries contribute in a crucial way to the electrical properties of colossal magnetoresistance (CMR) materials,[11] there is no microscopic information on the magnetic and electronic properties of the grain boundaries themselves. Here, we provide such information in the form of temperature (T)-dependent images obtained by magnetic force microscopy (MFM), which has a much higher resolution (30 nm) than other magnetic microscopies used to study manganites.[12–14] The images lead to the discovery of mesoscale regions around the grain boundaries which have magnetic, and therefore also electronic, properties different from those away from the grain boundaries. Apart from yielding an essential fact about thin transition metal oxide films, which are important both scientifically and technologically (especially where microelectronic applications are concerned), our work is significant as a demonstration of the use of force microscopy for discovering a spatially inhomogeneous temperature-dependent magnetic phenomenon.

We prepared our samples via the same procedures used to prepare the material for the grain boundary magnetotransport devices.[8,10] Epitaxial $La_{1-x}Sr_xMnO_3$ films with $x=0.3$ and 0.23 were grown by pulsed laser deposition on bicrystal $SrTiO_3(001)$ substrates with an artificial grain boundary where the crystals are misaligned by 45°. On one side of the artificial grain boundary the [100] crystal axis of $SrTiO_3$ crystal is parallel to the grain boundary, whereas on the other side, the [100] axis is rotated by 45° with respect to the grain boundary. The films are 100 nm thick. Because the lattice constant of $SrTiO_3$ is larger than that of $La_{1-x}Sr_xMnO_3$, the films grown on $SrTiO_3$ are subject to tensile strain, resulting in a suppression of the Curie temperature (T_c) compared to the bulk[15] and a magnetization vector M lying in the plane of the film.[16] We confirmed the in-plane orientation of M by measuring hysteresis loops at 300 K with the field H in the plane of the sample using a superconducting quantum interference device (SQUID) magnetometer (see the inset of Fig. 1). M as a function of T was measured for the film composition $x=0.3$ and its corresponding target material (Fig. 1). T_c for the film and the target material are 350 and 373 K, respectively, with the target material displaying a T_c which is 23 K higher than that of the film.

We used MFM to image the magnetic domain patterns in our films. The microscope was operated in the tapping mode where the phase shift ϕ of the oscillating cantilever was detected as the tip was scanned at a fixed height above the sample. The magnetic tips were magnetized along the long axis of the tips, which is perpendicular to the film plane. All the scans were done for zero external field. Since the films have an in-plane easy axis, the MFM will be sensitive to the regions where the magnetization vector is rotating, or, in other words, the magnetic domain walls. Panel (b) of Fig. 2 shows a typical magnetic domain pattern for the $La_{0.77}Sr_{0.23}MnO_3$ film around the artificial grain boundary. Panel (a) is the corresponding atomic force microscope (AFM) image, which attests both to the sharpness of the domain wall as well as the smoothness ($\lesssim 1$ nm root mean square (RMS) variation in thickness over a 20×20 μm^2 area) of the film. We can clearly see a sharp magnetic domain wall that coincides with the artificial grain boundary. In addition, there are magnetic domain walls on opposite sides of the grain boundary which are not nucleated along any feature visible in the AFM image. Although they meet at the artificial grain boundary, they have different orientations on either side, which represent the crystal orientation of the underlying substrate and consequently that of the film itself. On the left side of the grain boundary, the domain walls are parallel or perpendicular to the grain boundary. From the right side of the grain boundary, a magnetic domain wall initially emanates at an angle of 45° relative to the grain boundary. Because a 45° angle also characterizes the rotation of the crystal axes across the grain boundary in the bicrystal substrate, this confirms that our $La_{0.77}Sr_{0.23}MnO_3$ film is epitaxial and a bicrystal with an artificial grain boundary coincident with that of the bicrystal substrate. The magnetization vectors of the magnetic domains in the film are coupled to the crystal axes of the substrate—as we cross the grain boundary the magnetization vector has to rotate, and therefore it is natural to form a magnetic domain wall at the grain boundary. Figure 2 shows large magnetic domains at room temperature. Their sidelengths are of order 50 μm, much larger than the 100 nm film thickness.

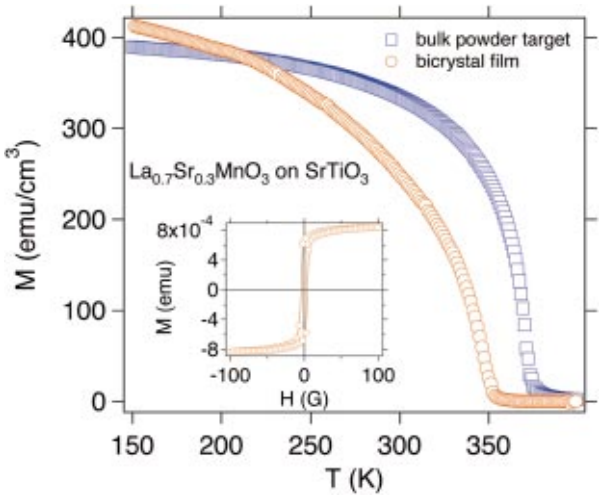

FIG. 1. (Color) M versus T of $La_{0.7}Sr_{0.3}MnO_3$ film and bulk powder sample. For the film, H was 20 G ($>$ coercive field) and was applied in the plane of the sample and perpendicular to the grain boundary. For the bulk powder sample which had a needle shape, H was 500 G and was applied along the long axis of the sample. The T_c of the film is 350 K, which is 23 K lower than the $T_c = 373$ of the powder target material. The inset shows the magnetic hysteresis loop of the film at 300 K, with the field applied in the plane of the film and perpendicular to the grain boundary.

We established the evolution of magnetic domains as a function of T for an $x = 0.3$ bicrystal film by imaging the domains using the MFM with the sample mounted on a variable temperature sample stage.[17] As shown in the left column of Fig. 3, raising T towards $T \simeq T_c$ [panel (b)] reduces the magnetic contrast which exists at room temperature [panel (a)]. As we increase T further, above T_c, we notice a remarkable thing—the emergence of a magnetic region [indicated by blue in panel (c)], very different from the domain pattern observed below T_c. Specifically, at 355 K, there is a distinct mesoscale region along the grain boundary, with a half width of approximately 0.7 μm. At $T = 360$ K, the mesoscale region shrinks to a half width of 0.5 μm and it disappears entirely at $T = 370$ K. The effect is observed not only at the artificial grain boundary (which was introduced intentionally) but also at other locations on the film (see right column of Fig. 3), where there are naturally occurring substrate defects. These defects can be clearly seen in the topography (AFM) channel. In such a location, we followed the evolution of the magnetic images in smaller T increments. The T dependence of the new magnetic region is the same as that around the artificial grain boundary. It appears at $T \gtrsim T_c$, peaks at 360 K, and vanishes at 370 K.

To quantify the magnetic contrast, we calculated the RMS of ϕ in the MFM image at each temperature, where $\phi_{\mathrm{rms}} = \sqrt{\langle [\phi(x,y) - \phi_{\mathrm{av}}]^2 \rangle}$. $\phi(x,y)$ represents the phase shift at each pixel and ϕ_{av} is the average phase shift in the MFM image. The results are plotted in Fig. 4(c). The magnetic contrast between the mesoscale region [indicated by blue in panels (c), (d), (g), and (h)] and the rest of the sample [indicated by yellow and green in (c), (d), (g), and (h)] arises because the mesoscale region is ferromagnetic (FM) and the

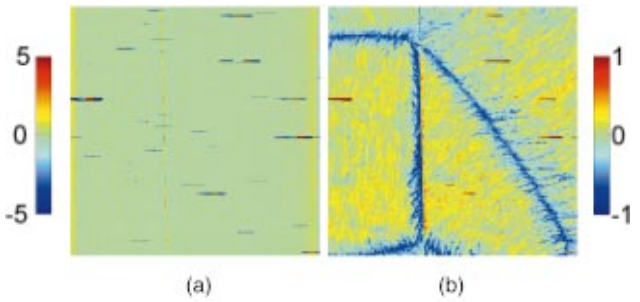

FIG. 2. (Color) Room temperature AFM and MFM images of the region around the artificial grain boundary in the $La_{0.77}Sr_{0.23}MnO_3$ film grown on a bicrystal $SrTiO_3(001)$ substrate. The scan size is 74 μm for both images. (a) The AFM image shows the topography of the film, which indicates the presence of an artificial grain boundary. The z scale is in units of nm. (b) The MFM image displays the magnetic domain walls in the system, one of which coincides with the artificial grain boundary. The z scale represents the phase shift of the oscillating cantilever in degree units.

rest is paramagnetic (PM) at $T \gtrsim T_c$. When both the mesoscopic region and the bulk part of the film are ferromagnetic (when $T < T_c$, i.e., at 300 K), the magnetization vector has a large magnitude, and therefore the interaction between the tip and the sample is strong, resulting in a large magnetic contrast in the MFM image at regions where the magnetization vector rotates (i.e., at the domain walls). When the film becomes weakly ferromagnetic (when $T \sim T_c$), the interaction between the tip and the sample is weak all across the sample. Therefore, the variation of ϕ across the scanned image is small resulting in a small ϕ_{rms}. As the ferromagnetism of the bulk part vanishes, the difference in magnetic force between the mesoscopic region (ferromagnetic) and the rest of the sample (paramagnetic) increases, giving rise to a large variation of ϕ across the image and resulting in a large ϕ_{rms} as shown in Fig. 4(c). Eventually, the difference in magnetic force between the two regions decreases and vanishes as the ferromagnetism of the mesoscopic region vanishes and the whole film becomes paramagnetic.

It is notable that the magnetic regions above T_c are magnetized in one direction when imaged with the MFM (as evidenced by the dominant blue color in the images) and the force between the tip and these ferromagnetic regions is always attractive. We believe that the tip magnetizes these regions in a direction perpendicular to the film plane as it scans the sample. This is likely to happen given that these regions are isotropic soft magnets with a small coercive field ($H_c \lesssim 8$ G), as described below and shown in Fig. 4(b). From the images, T_c can be mapped spatially by locating the ferromagnetic–paramagnetic boundary as a function of T since at the boundary $T = T_c$ [Fig. 4(a)]. That the mesoscopic regions shrink as T is raised shows that T_c varies spatially, with the regions closer to the grain boundary having a higher T_c.

We have discovered that a thin manganite film has inhomogeneous magnetic properties due to both natural and artificial grain boundaries. Because the grain boundaries, especially when the micron scale healing length observed directly

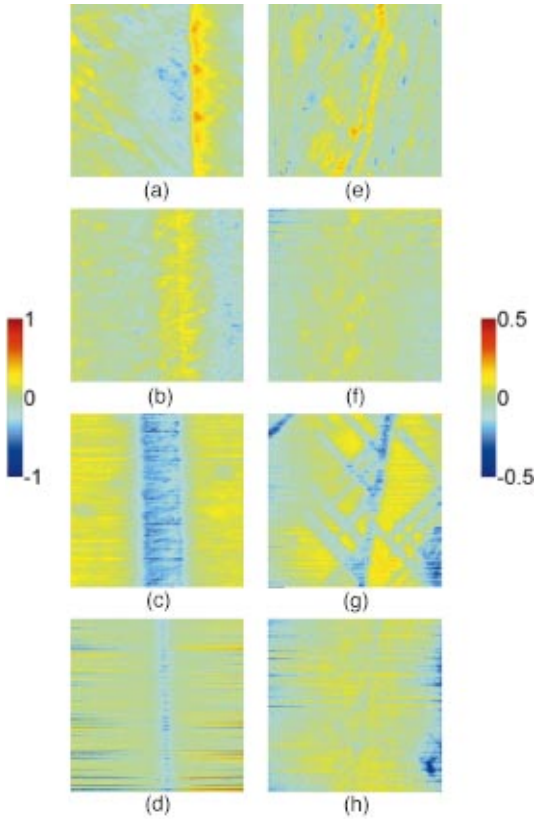

FIG. 3. (Color) The evolution of the magnetic pattern in the $La_{0.7}Sr_{0.3}MnO_3$ film around the artificial grain boundary and around natural defects as a function of T. Images (a), (b), (c), and (d) were taken around the artificial grain boundary at 300, 350, 355, and 365 K, respectively. The scan size for these images was 5 μm and a common z scale was used, which is displayed at the left of the images in degree units. Images (e), (f), (g), and (h) display the magnetic pattern around natural defects at 300, 350, 355, and 365 K, respectively. The scan size for this region was 14 μm. The z scale for the scans is displayed at the right of the image in degree units. As T is raised from 300 K, the magnetic contrast diminishes. As T is raised above T_c, a magnetic region emerges around the grain boundary. The width and strength of this magnetic region evolves as a function of T. The region eventually vanishes at $T=370$ K.

in the MFM images is taken into account, occupy an appreciable volume of the film, we expect to see evidence for ferromagnetism extending up to 370 K in very sensitive bulk magnetization measurements. Therefore, we have measured hysteresis loops using SQUID magnetometry. Indeed, we found that although the temperature dependence of the order parameter indicates a $T_c=350$ K for $x=0.3$ film composition, there is still a tiny hysteresis left at $T\gtrsim T_c$ [see Fig. 4(b)]. The tiny hysteresis loops close exactly at the same temperature ($T=370$ K) at which the mesoscale regions disappear in the MFM image. The hysteresis loops at $T\gtrsim T_c$ have the same shape whether the field is applied in the plane or perpendicular to the plane of the film. This indicates that the ferromagnetic regions around the grain boundaries are isotropic, in contrast to the rest of the film, which shows an in-plane easy axis throughout the whole temperature

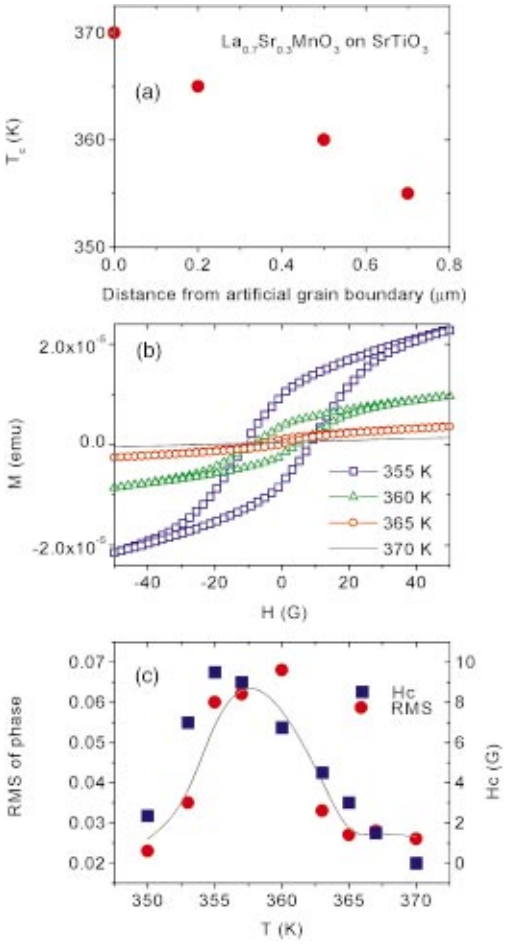

FIG. 4. (Color) Comparison between magnetic information derived from MFM measurements and standard bulk magnetometry data. (a) Dependence of T_c on the distance from the artificial grain boundary, as established from the MFM images in Fig. 3. (b) Magnetic hysteresis loops of the $La_{0.7}Sr_{0.3}MnO_3$ film for $T>T_c$ were measured with the magnetic field applied in the plane of the film and perpendicular to the artificial grain boundary. The loops, which are open at $T<370$ K, close at 370 K. (c) Left axis shows the magnetic contrast of the MFM images in Fig. 3 represented by the RMS of ϕ in the MFM signal as a function of T. This is compared against the quantity plotted on the right axis, which is the coercive field H_c of the $La_{0.7}Sr_{0.3}MnO_3$ film at $T>T_c$ extracted from the magnetic hysteresis loops in panel (b). The solid line is a smooth fit of the RMS of ϕ and serves as a guide to the eye. The T dependence of H_c above T_c has a similar T dependence as $\phi_{\rm rms}$ for following similar reasons. The measured magnetization is the superposition of a hysteretic contribution from the FM GB regions and a nonhysteretic term due to the rest of the film, which is PM. For $T\sim T_c$, the second term will dominate because of the high susceptibility of the PM film, with the result that the apparent H_c, defined as the field where M crosses zero in the M vs H loop will be much suppressed relative to the coercive field H_c^{GB} which would be measured for the FM GB regions by themselves. As T is increased and the PM susceptibility drops, the observed H_c would rise to approach H_c^{GB}. Eventually though H_c^{GB} itself will drop as the GB ferromagnetism disappears, pulling H_c down as well. The outcome is then that H_c will display a maximum somewhere between the T_c of the bulk film and the maximum T_c for the GB's, which of course is precisely what we observe.

range including the vicinity of T_c. The isotropic magnetic phase at $T>T_c$, explains why it is easy to align the moments perpendicular to the plane with the field exerted by the MFM tip.

We also measured magnetization loops in the bulk powder (ceramic) target $La_{0.7}Sr_{0.3}MnO_3$ from which the film was grown. Hysteresis ceases at 370 K, which is also the Curie temperature deduced from M versus T data (see Fig. 1). Therefore, in the bulk ceramic sample, which has a large number of grain boundaries, we do not detect regions with local T_c higher than the nominal T_c of the sample. This means that the presence of grain boundaries as they exist in the ceramic is not sufficient for the observation of a higher local T_c. If we compare the magnetization per unit volume for the film to that of the bulk powder target for temperatures above T_c of the film, we can estimate the volume fraction of the film which is ferromagnetic at these temperatures. At $T=355$, 360, and 365 K, which are intermediate between the nominal Curie temperatures of the film and the powder, the ferromagnetic volume fractions are 0.03, 0.02, and 0.01, respectively. These values are consistent with an estimate ($0.02=1$ μm width/50 μm distance between grain boundaries) of the volume fraction occupied by mesoscale ferromagnetic regions in the film, and so indicate that the small ''foot'' in $M(T)$ above T_c for the film (see Fig. 1) is actually due to grain boundary magnetism. Almost needless to say, in the absence of our MFM data, the foot would have many possible interpretations.

We attribute the variation of local T_c to the variation of strain in the film. The effect of strain on the T_c of CMR films has been reported by various groups[18–20] and is by now a well-accepted phenomenon. Depending on the lattice mismatch between the film and the substrate, the strain on the film can be modulated, which in turn modulates T_c substantially. This phenomenon has been attributed to the Jahn-Teller distortion arising from biaxial strain.[18] The coincidence of Curie temperatures (the ceramic T_c and the maximum local T_c at the defects) and the magnetization per unit volume make it very likely that the mesoscale regions in our films are very similar to the bulk starting material. Therefore, near the grain boundaries, the film is strain relieved leading to a T_c almost the same as that of the bulk. On the other hand, away from these crystal imperfections, the film is under tensile strain and its T_c is suppressed by 20 K. The width of the mesoscale region is an indication of the range over which strain propagates from the grain boundary.

To summarize, we have discovered distinctive magnetic properties—most notably a higher Curie temperature—in mesoscale regions around grain boundaries in manganites. The distinctive properties obtain whether the grain boundaries occur naturally in unplanned fashion, or are introduced deliberately via a bicrystal substrate. They therefore need to be incorporated in descriptions of the electronic transport in all CMR films. Instead of sharp boundaries that divide crystal grains, one needs to consider separate regions around the grain boundaries, which may have not only different magnetic properties, but also different electronic structures. A magnetically disordered region or mesoscale region around the grain boundaries has been invoked[4,5,7] to explain magnetotransport results, which could not be explained by spin-polarized tunneling at a sharp interface. Our results represent direct evidence that the interfaces have magnetic properties which are actually modulated over mesoscopic distances. Beyond its implications for a topic of great current interest, namely exploiting grain boundaries for electronic devices, our experiment is significant because it is pioneering in the sense of imaging a spatially varying Curie temperature and using force microscopy as a quantitative tool in the study of a temperature-dependent magnetic phenomenon.

We are very grateful to Peter Littlewood for helpful discussions and the contacts which made this collaboration possible, as well as to Chang-Yong Kim for valuable x-ray analysis of our films.

[1] H.L. Ju *et al.*, Phys. Rev. B **51**, 6143 (1995).
[2] P. Schiffer *et al.*, Phys. Rev. Lett. **75**, 3336 (1995).
[3] H.Y. Hwang *et al.*, Phys. Rev. Lett. **77**, 2041 (1996).
[4] A. Gupta *et al.*, Phys. Rev. B **54**, R15 629 (1996).
[5] J.E. Evetts *et al.*, Philos. Trans. R. Soc. London, Ser. A **356**, 1593 (1998).
[6] L. Balcells *et al.*, Phys. Rev. B **58**, R14 697 (1998).
[7] J. Klein *et al.*, Europhys. Lett. **47**, 371 (1999).
[8] N.D. Mathur *et al.*, Nature (London) **387**, 266 (1997).
[9] K. Steenbeck *et al.*, Appl. Phys. Lett. **71**, 968 (1997).
[10] S.P. Isaac *et al.*, Appl. Phys. Lett. **72**, 2038 (1998).
[11] S. Jin *et al.*, Science **264**, 413 (1994).
[12] P. Lecoeur *et al.*, J. Appl. Phys. **82**, 3934 (1997).
[13] D.K. Petrov *et al.*, J. Appl. Phys. **83**, 7061 (1998).
[14] Z.W. Lin *et al.*, Appl. Phys. Lett. **74**, 3014 (1999).
[15] F. Tsui *et al.*, Appl. Phys. Lett. **76**, 2421 (2000).
[16] C. Kwon *et al.*, J. Magn. Magn. Mater. **172**, 229 (1997).
[17] Y. Soh and G. Aeppli, J. Appl. Phys. **85**, 4607 (1999).
[18] A.J. Millis, T. Darling, and A. Migliori, J. Appl. Phys. **83**, 1588 (1998).
[19] Q. Gan *et al.*, Appl. Phys. Lett. **72**, 978 (1998).
[20] R.A. Rao *et al.*, J. Appl. Phys. **85**, 4794 (1999).